Searching for the *CP*-odd Higgs boson of the minimal supersymmetric model at hadron supercolliders

John F. Gunion
Department of Physics, University of California, Davis, California 95616

Howard E. Haber
Santa Cruz Institute for Particle Physics, University of California, Santa Cruz, California 95064

Chung Kao
Department of Physics, B-159, Florida State University, Tallahassee, Florida 32306

(Received 7 February 1992)

The *CP*-odd Higgs boson A^0 of a nonminimal Higgs model possesses no tree-level couplings to vector-boson pairs. As a result, many of the techniques employed to search for the standard model Higgs boson at the Superconducting Super Collider (SSC) and CERN Large Hadron Collider (LHC) are not likely to be useful in searches for the A^0. This paper focuses on the phenomenology of A^0 production and decay in the minimal supersymmetric model. We evaluate a comprehensive set of branching ratios for A^0 (which includes all two-body tree-level and one-loop decays into nonsupersymmetric final states), including the effects of leading-log radiative corrections. The one-loop decay $A^0 \to ZZ$ leads to the "gold-plated" signature $ZZ \to l^+l^-l^+l^-$ and provides an observable signature for A^0 production at the SSC and LHC only over a very narrow region of parameter space. More promising signatures for the A^0 are also discussed.

PACS number(s): 14.80.Gt, 12.15.Cc, 13.85.Qk, 14.80.Ly

I. INTRODUCTION

Future hadron supercolliders such as the Superconducting Super Collider (SSC) and CERN Large Hadron Collider (LHC) will provide an ideally suited laboratory for the search for the standard model Higgs boson. (For a comprehensive review and guide to the literature see Ref. [1]; newer developments are surveyed in Refs. [2,3,4].) However, various theoretical arguments suggest that the sector responsible for electroweak symmetry breaking will be more complicated. Among the theoretical approaches which go beyond the standard model, the supersymmetric extension of the standard model is particularly attractive in that it preserves the elementary nature of the Higgs bosons [5]. In the minimal supersymmetric model (MSSM), the Higgs sector consists of a two-doublet extension of the standard model in which two Higgs-sector parameters suffice in fixing the properties of the physical Higgs bosons [1,6,7].

In models with a nonminimal Higgs sector, there are additional Higgs scalars beyond the neutral *CP*-even Higgs boson of the minimal standard model. In the absence of *CP* violation in the Higgs potential, the neutral Higgs scalars can be characterized as either *CP* even or *CP* odd[1]. In Refs. [8], and [9], we surveyed the properties of the *CP*-even Higgs scalars and evaluated the prospects for their detection at hadron supercolliders. In this paper, we focus on the phenomenology of the *CP*-odd scalar (which we denote by A^0). Present experimental data from the CERN e^+e^- collider LEP [10] indicate that $m_A \gtrsim 40$ GeV (in the context of the MSSM). This mass limit is obtained primarily by the failure to observe the A^0 in $Z \to h^0 A^0$ (where h^0 is the lightest *CP*-even Higgs boson).[2] Presumably, this mass limit will improve by about a factor of 2 after LEP-II completes its experimental search for $e^+e^- \to Z^* \to h^0 A^0$. In this paper, we examine some of the issues involved in the search for the A^0 at a hadron supercollider.

The key property of the A^0 that makes it difficult to detect at e^+e^- and hadron colliders is the absence of a tree-level A^0VV vertex (where $V = W^\pm$ or Z). For example, at e^+e^- colliders, the *CP*-even Higgs boson h^0 is produced via the associated production of h^0 and a (real or virtual) Z. At higher energies, WW fusion to h^0 becomes significant. Both of these production modes are

[1]The Higgs sector of the MSSM is automatically *CP* conserving.

[2]In the MSSM, m_A and $\tan\beta$ are sufficient to fix all tree-level properties of the Higgs sector. Thus, nonobservation of h^0 (whose mass depends on m_A and $\tan\beta$) and A^0 at LEP determines a lower bound on m_A (which depends weakly on $\tan\beta$). The limit $m_A \gtrsim 40$ GeV holds for $\tan\beta \gtrsim 1.1$; however, the 95% confidence level limit of ALEPH independent of $\tan\beta$ is $m_A \geq 20$ GeV. In an arbitrary two-Higgs-doublet model, the nonobservation of h^0 and A^0 does not uniquely fix an experimental lower bound for m_A. For example, if h^0 were heavier than the Z, then no A^0 production process would have been observed at LEP to date.

unavailable to the A^0. The production of h^0A^0 (via Z exchange) is probably the only realistic mechanism for A^0 discovery [11]. At a hadron supercollider, the production of A^0 is less problematical. As we shall demonstrate in Sec. IV, gluon-gluon fusion into A^0 or $A^0Q\bar{Q}$ (where $Q=t$ or b quark) provides an ample event sample at the SSC (and LHC). At hadron supercolliders, the major problem in the A^0 search involves its detection above background. For example, if 150 GeV $\lesssim m_{\phi^0} \lesssim$ 800 GeV (where ϕ^0 is the standard model Higgs boson), then the ϕ^0 can be easily discovered via its "gold-plated" mode: $\phi^0 \to ZZ \to l^+l^-l^+l^-$ [1]. Many other Higgs-boson decay signatures also rely on the Higgs-boson coupling to ZZ or W^+W^-. Naively, these mechanisms are unavailable to the A^0 search due to the absence of a tree-level A^0VV coupling.

In Sec. II, we compute the one-loop decays of $A^0 \to VV$ and examine whether they are phenomenologically relevant for the search for A^0 at the SSC and LHC. Explicit formulas are given for the decay widths of A^0 into $\gamma\gamma$, $Z\gamma$, W^+W^-, and ZZ. For simplicity, we only include the effects of standard model particles in the loops. (The effects of supersymmetric particles are generally small if the effective supersymmetry breaking scale is somewhat above the electroweak scale.) In Sec. III, we evaluate the branching ratios of A^0 into two-body final states. In an arbitrary two-Higgs-doublet model, the decay rate for $A^0 \to Zh^0$ is generally large and proportional to the Higgs sector parameter $\cos^2(\beta-\alpha)$ which is independent of the parameters that determine the A^0 production rate and its decay into VV and $Q\bar{Q}$. In contrast, in the MSSM, $\cos^2(\beta-\alpha)$ is suppressed over most of the parameter space, so that the rate for $A^0 \to Zh^0$ is sufficiently reduced to allow for a non-negligible rate for $A^0 \to VV$ if $m_A < 2m_t$. In Sec. IV, we evaluate the production cross sections for A^0 at the SSC and LHC. By folding in the branching ratio for $A^0 \to ZZ$ followed by Z leptonic decays, we obtain the number of four-charged-lepton events from A^0 decay in an SSC (and LHC) year. Although the number of four-lepton events is generally meager, there does exist a very limited range of parameter space in which such events could be seen. In Sec. V, we make some brief comments on the phenomenological relevance of other A^0 decay channels, and indicate the direction of future work. Complementary work on the phenomenology of Higgs bosons of the MSSM at hadron supercolliders has recently appeared in Ref. [12].

II. ONE-LOOP A^0 DECAYS INTO VECTOR-BOSON PAIRS

In this section, we compute the one-loop matrix element for $A^0 \to VV$, where the loop consists of a fermion which couples diagonally to the A^0 with a pseudoscalar (γ_5) coupling. We take the fermion coupling to V to be an arbitrary combination of vector and axial vector. As a result, we can apply our results to A^0 decay to W^+W^-, ZZ, $Z\gamma$, and $\gamma\gamma$ [13]. Note that this is not the most general computation of one-loop A^0 decay to VV. For example, in order to include supersymmetric fermions (e.g., neutralinos and charginos) in the loop, one would have to allow for the possibility of a nondiagonal coupling of A^0 to $\tilde{\chi}_i\tilde{\chi}_j$ with an arbitrary mixture of scalar and pseudoscalar coupling at the $A^0\tilde{\chi}_i\tilde{\chi}_j$ vertex. We shall not present this more general computation in this paper. At the end of this section, we will argue that the contributions of supersymmetric loops is expected to be rather small (compared to the fermion loops included below). Thus, in an initial investigation, it makes sense to neglect the supersymmetric contributions.

The reader may wonder whey we do not include gauge-boson and Higgs-boson loops. It is easy to see that the sum of such contributions must exactly cancel. In the bosonic sector, the electroweak theory separately conserves P and C. It is straightforward to check that a consistent assignment of C-quantum numbers implies that A^0, Z, and γ are all C odd [14]. In addition, the CP-odd, zero angular momentum state of W^+W^- must be C even [15]. Thus, no A^0VV coupling exists to all orders in the bosonic sector of the theory. This conclusion remains true if we add squarks and sleptons to the model.[3] Of course, when we add fermions to the electroweak theory, C and P are separately violated. Thus, fermion loops *can* mediate $A^0 \to VV$ as discussed above.

Consider the process

$$A^0(k) \to V_i(k_1) + V_j(k_2) , \tag{1}$$

where the respective four-momenta are indicated in parentheses. Since A^0 is a CP-odd scalar, the invariant amplitude for the decay takes the simple form

$$\mathcal{M}(A^0 \to V_iV_j) = (1+S_{ij}) \frac{g^3 N_c}{16\pi^2 m_W} \epsilon_{\mu\nu\alpha\beta} \varepsilon_1^\mu \varepsilon_2^\nu k_1^\alpha k_2^\beta \mathcal{A} , \tag{2}$$

where $S_{ij}=0$ for W^+W^- and $S_{ij}=1$ for all neutral V_iV_j combinations, and the number of colors, $N_c=3(1)$ for a quark (lepton) internal loop. The factor $(1+S_{ij})$ is present since in the case of neutral final state bosons there are two inequivalent triangle diagrams for a given fermion loop. Explicit expressions for $\mathcal{A}$ will be given below for the various final state vector bosons. The partial decay rate for process (1) is

$$\Gamma(A^0 \to V_iV_j) = \frac{(1+S_{ij})^2}{(1+\delta_{ij})} \frac{g^6 N_c^2 \lambda^{3/2}}{2^{13}\pi^5 m_W^2 m_A^3} |\mathcal{A}|^2 , \tag{3}$$

where $\lambda \equiv (m_A^2 - m_{V_i}^2 - m_{V_j}^2)^2 - 4m_{V_i}^2 m_{V_j}^2$. Note that the above formula includes a factor of $\frac{1}{2}$ in the case of identical final state bosons.

To compute $\mathcal{A}$, we must sum over the loop diagrams shown in Fig. 1. Note that the Lorentz structure of the individual graphs of Fig. 1 need not be of the form exhib-

[3] It is easy to check explicitly that the one-loop Feynman graphs contributing to $A^0 \to \tilde{q}_1\bar{\tilde{q}}_2 \to VV$ and $A^0 \to \tilde{q}_2\bar{\tilde{q}}_1 \to VV$ exactly cancel in pairs (where $\tilde{q}_i$ are the squark mass eigenstates). This cancellation occurs because the Feynman rule for $A^0 \to \tilde{q}_i\bar{\tilde{q}}_j$ changes sign when i and j are interchanged.

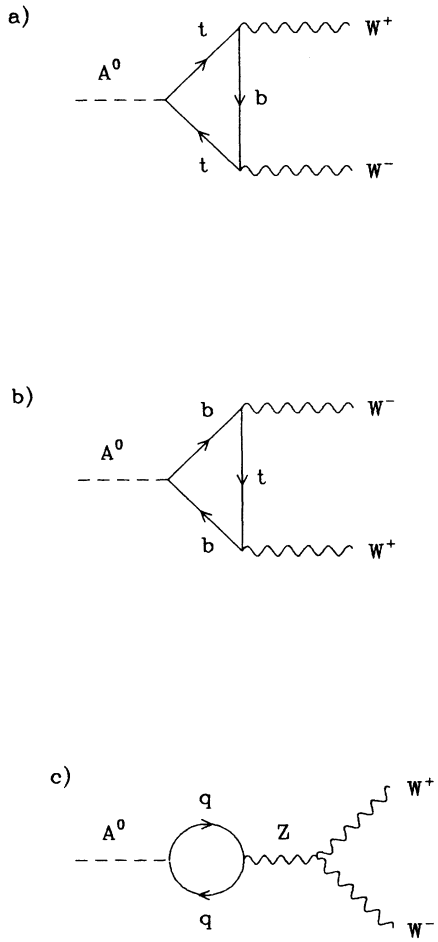

FIG. 1. Quark-loop graphs for $A^0 \to W^+W^-$. Graph (c) is identically zero for onshell W bosons. (This is most easily seen in the Landau gauge.) In the case of $A^0 \to VV$, $V = Z$ or γ, graph (c) is absent, and graphs (a) and (b) (where the internal fermion flavor is fixed) are equal, as they differ only by the exchange of two identical external boson lines.

ited in Eq. (2). However, it is easy to check that the total amplitude is of the required form. The results for $V = W^{\pm}$, Z, and γ can be obtained simultaneously by writing the $Vf\bar{f}'$ vertex as

$$-ig\left[G_f^L\left[\frac{1-\gamma_5}{2}\right]+G_f^R\left[\frac{1+\gamma_5}{2}\right]\right], \tag{4}$$

where G^L and G^R are given in Table I.

TABLE I. Left- and right-handed couplings of V to fermion pairs. An overall factor of $-ig$ is not included above. $T_3 = \pm\frac{1}{2}$ is the third component of weak isospin and Q is the fermion charge in units of $e > 0$.

V	G^L	G^R
$W^{\pm}$	$1/\sqrt{2}$	0
Z	$(T_3 - Q\sin^2\theta_W)/\cos\theta_W$	$-Q\sin^2\theta_W/\cos\theta_W$
γ	$Q\sin\theta_W$	$Q\sin\theta_W$

For the $A^0 f\bar{f}$ vertex, we assume a Higgs-fermion coupling in which one Higgs doublet couples only to down-type fermions and the other Higgs doublet couples only to up-type fermions. (This is the coupling pattern in the MSSM.) The resulting Feynman rules are

$$g_{A^0 t\bar{t}} = \frac{-gm_t\cot\beta}{2m_W}\gamma_5 ,$$
$$g_{A^0 b\bar{b}} = \frac{-gm_b\tan\beta}{2m_W}\gamma_5 . \tag{5}$$

The final result for $\mathcal{A}$ can be expressed in terms of two functions $\mathcal{C}$ and $\mathcal{I}$, which are defined in terms of the 't Hooft–Veltman loop functions [16]. The relevant definitions can be found in the Appendix. The contribution of one generation of quarks to $\mathcal{A}$ is (using third generation notation)

$$\mathcal{A}(A^0 \to V_i V_j) = m_t^2\cot\beta\,\mathcal{A}_t + m_b^2\tan\beta\,\mathcal{A}_b , \tag{6}$$

where $\mathcal{A}_t$ and $\mathcal{A}_b$ are given below for the following cases.

(i) $A^0 \to W^+W^-$:

$$\mathcal{A}_t = \tfrac{1}{2}[\mathcal{C}(m_W^2;m_t^2,m_b^2)+\mathcal{I}(m_W^2;m_t^2,m_b^2)] ,$$
$$\mathcal{A}_b = \tfrac{1}{2}[\mathcal{C}(m_W^2;m_b^2,m_t^2)+\mathcal{I}(m_W^2;m_b^2,m_t^2)] , \tag{7}$$

(ii) $A^0 \to VV$, for $V = Z$ or γ:

$$\mathcal{A}_f = ([G_f^L]^2+[G_f^R]^2)\mathcal{C}(m_V^2;m_f^2) + (G_f^L - G_f^R)^2\mathcal{I}(m_V^2;m_f^2) , \tag{8}$$

(iii) $A^0 \to Z\gamma$:

$$\mathcal{A}_f = Q_f\sin\theta_W(G_f^L+G_f^R)\mathcal{C}(m_Z^2,0;m_f^2) . \tag{9}$$

In (ii) above, one must use the G^L and G^R of Table I appropriate for Z or γ, while in (iii) one must use the corresponding Z couplings.

In the Appendix, we give asymptotic forms for $\mathcal{C}$ and $\mathcal{I}$ in the limit of large m_t. Because these functions scale as $1/m_t^2$ in this limit, we see that $\mathcal{A}$ approaches a constant as $m_t \to \infty$. Furthermore, we note that the terms proportional to m_b are negligible except for the case of very large $\tan\beta$, in which case the b-quark contribution can compete with that of the t quark. The contributions from all other quarks and leptons are negligible. It is convenient to normalize the A^0 partial widths to

$$\Gamma(A^0 \to b\bar{b}) \simeq \frac{g^2N_c m_A m_b^2\tan^2\beta}{32\pi m_W^2} . \tag{10}$$

We are interested in the regime where $m_A \gg m_b$, so we have set $m_b = 0$ in the phase space factor. Keeping only the t-quark contribution to the one-loop amplitude, we obtain the following simple expressions which are valid when $m_t \gg m_A$:

$$\frac{\Gamma(A^0 \to W^+W^-)}{\Gamma(A^0 \to b\bar{b})} \simeq \frac{3\alpha^2 m_A^2\cot^4\beta}{256\pi^2 m_b^2\sin^4\theta_W}\left[1-\frac{4m_W^2}{m_A^2}\right]^{3/2} , \tag{11}$$

$$\frac{\Gamma(A^0\to ZZ)}{\Gamma(A^0\to b\bar{b})}\simeq\frac{3\alpha^2 m_A^2\cot^4\beta}{128\pi^2 m_b^2}\left[\frac{1-4\sin^2\theta_W+\frac{16}{3}\sin^4\theta_W}{3\sin^2\theta_W\cos^2\theta_W}\right]^2\times\left[1-\frac{4m_Z^2}{m_A^2}\right]^{3/2},\tag{12}$$

$$\frac{\Gamma(A^0\to Z\gamma)}{\Gamma(A^0\to b\bar{b})}\simeq\frac{\alpha^2 m_A^2\cot^4\beta}{48\pi^2 m_b^2}\times\left[\frac{1-\frac{8}{3}\sin^2\theta_W}{\sin\theta_W\cos\theta_W}\right]^2\left[1-\frac{m_Z^2}{m_A^2}\right]^3,\tag{13}$$

$$\frac{\Gamma(A^0\to\gamma\gamma)}{\Gamma(A^0\to b\bar{b})}\simeq\frac{2\alpha^2 m_A^2\cot^4\beta}{27\pi^2 m_b^2}.\tag{14}$$

These expressions are useful since they provide a reasonable estimate even when $m_A\sim m_t$.

In the computation of the amplitude $\mathcal{A}$ above, we omitted the possibility of supersymmetric particles (charginos and neutralinos) which can also appear in the loops.[4] However, in contrast with the calculation above (where $\mathcal{A}$ approaches a constant value in the limit of $m_t\gg m_A$), the contribution of supersymmetric particles smoothly decouples for $M_{\rm SUSY}\gg m_A$. (Here, we use $M_{\rm SUSY}$ to generically denote the mass scale which characterizes supersymmetric particle masses.) This result can be explicitly seen in the formulas for $A^0\to\gamma\gamma$ given in Appendix C of Ref. [1] and in Ref. [17]. The supersymmetric contributions to $A^0\to Z\gamma$ (as well as $A^0\to\gamma\gamma$) are also given in Ref. [18].

III. BRANCHING RATIOS OF THE *CP*-ODD HIGGS BOSON IN THE MSSM

In order to compute the A^0 branching ratios, we need to evaluate the partial decay rates of A^0 into its most important channels. If $m_A<2m_t$, then the two most important channels are $A^0\to b\bar{b}$ and $A^0\to Zh^0$ (where h^0 is the lightest *CP*-even Higgs scalar). The decay rate into $b\bar{b}$, given in Eq. (10) above, is the tree-level result. In our numerical results which we present below, we shall also include the QCD corrections to this result which roughly reduces the tree-level prediction by a factor of 2, which is mostly attributable to the running of the b-quark mass from $2m_b$ to the Higgs-boson mass [19]. The decay rate into Zh^0 is given by [20]

$$\Gamma(A^0\to Zh^0)=\frac{g^2\lambda^{3/2}\cos^2(\beta-\alpha)}{64\pi m_Z^2 m_A^3\cos^2\theta_W},\tag{15}$$

where $\lambda\equiv(m_A^2-m_Z^2-m_h^2)^2-4m_Z^2m_h^2$. Thus, to obtain this decay rate, two new parameters are required: the lightest *CP*-even Higgs-boson mass, m_h and the *CP*-even Higgs mixing angle α. In a general two-Higgs-doublet model, these parameters would be independent of the Higgs parameters m_A and $\tan\beta$. In the MSSM, the Higgs sector is greatly constrained. At the tree level, the parameters m_A and $\tan\beta$ are sufficient to determine all other Higgs sector parameters. These relations can be significantly modified by electroweak radiative corrections if the top-quark mass is large [21–26]. In this case, m_h and $\cos(\beta-\alpha)$ should be considered as functions of m_A, $\tan\beta$, m_t, and the top-squark mass.

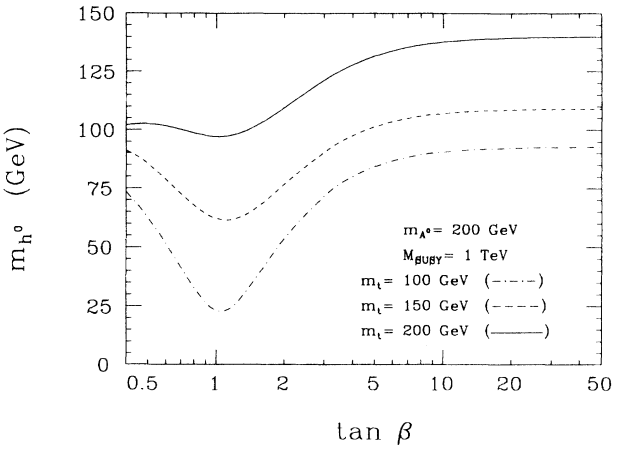

FIG. 2. The mass of the lightest *CP*-even Higgs scalar (h^0), including one-loop leading-log radiative corrections, as a function of $\tan\beta$, for $m_A=200$ GeV and $M_{\tilde{t}}=1$ TeV (squark mixing has been neglected). Dependence on m_A is rather weak as long as $m_A\gg m_h$. Curves are show for three different values of m_t.

At tree-level, $m_h\le m_Z|\cos 2\beta|$. Including one-loop radiative corrections, m_h acquires a large positive mass shift of order $(g^2m_t^4/m_Z^2)\ln(M_{\tilde{t}}^2/m_t^2)$, for $m_A>m_h$. In Fig. 2, we display m_h, including one-loop leading-log radiative corrections, for $m_A=200$ GeV and $M_{\tilde{t}}=1$ TeV and no squark mixing [26]. (The exact one-loop radiatively corrected mass differs from the displayed results by no more than a few GeV [27].) Note that for $m_A\gtrsim 200$ GeV, there is a substantial range of parameter space for which the decay $A^0\to Zh^0$ is kinematically allowed. However, Eq. (15) implies that the importance of this decay mode is critically dependent on the magnitude of $\cos^2(\beta-\alpha)$. The behavior of $\cos^2(\beta-\alpha)$ as a function of m_A for two different $\tan\beta$ values is shown in Fig. 3. Note that $\cos(\beta-\alpha)$ falls rapidly as m_A increases. This has a significant impact on the magnitude of the $A^0\to Zh^0$ branching ratio. From results quoted above,

$$\frac{\Gamma(A^0\to Zh^0)}{\Gamma(A^0\to b\bar{b})}=\frac{m_A^2\cos^2(\beta-\alpha)}{6m_b^2\tan^2\beta}\times[(1-r_Z-r_h)^2-4r_Zr_h]^{3/2},\tag{16}$$

where $r_a=m_a^2/m_A^2$. In a general two-Higgs-doublet model, there is no *a priori* reason for expecting $\cos^2(\beta-\alpha)$ to be especially small. In this case, $A^0\to Zh^0$ would be the dominant mode over essentially the entire range of m_A for which the decay is kinematically allowed. In contrast, in the MSSM, because of the large suppression of $\cos^2(\beta-\alpha)$ as shown in Fig. 3, $A^0\to Zh^0$ is no longer the dominant decay mode of the A^0, as will

[4]The total contribution of squark and slepton loops to the one-loop amplitude vanishes as discussed earlier in this section.

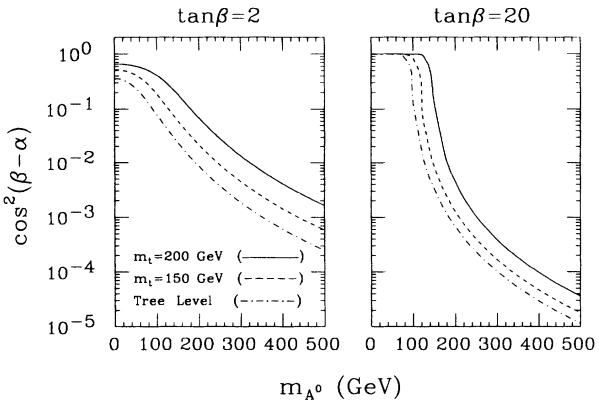

FIG. 3. The value of $\cos^2(\beta-\alpha)$ as a function of m_A for $\tan\beta=2$ and 20. The tree-level result is shown by the dashdot curve. The two other curves include the one-loop leading-log radiative corrections to $\cos(\beta-\alpha)$ with $m_t=150$ GeV (dashes) and $m_t=200$ GeV (solid), and $M_{\tilde{t}}=1$ TeV (squark mixing has been neglected).

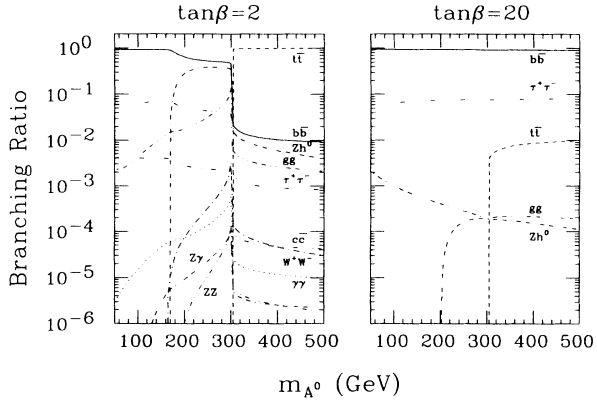

FIG. 4. Branching ratios for A^0 computed for $m_t=150$ GeV and for $\tan\beta=2$ and 20. One-loop radiative corrections have been included as described in the text. The notation for the curves follows: $b\bar{b}$ (——); $t\bar{t}$, (— — —); W^+W^-(—·—·—·); ZZ(··—··—); Zh^0(·——·——); $c\bar{c}$(···—); $\tau^+\tau^-$(····—); $\gamma\gamma$(· · · ·); $Z\gamma$(··— —); gg(··· — —).

be shown in detail below.

The procedure for obtaining the branching ratios of the A^0 in the MSSM is as follows. We shall assume that the mass scale characterizing supersymmetric particles lies above the electroweak scale. Specifically, we assume that the decay of A^0 into supersymmetric final states is kinematically forbidden, and that the contributions to one-loop-induced decays from supersymmetric particle loops are suppressed. Thus, we consider all possible non-supersymmetric two-body final states in A^0 decay. The basic tree-level formulas for the various decay rates can be found in Ref. [1]. We improve on these results by incorporating the complete leading-log one-loop electroweak radiative corrections in the calculation. First, we compute the leading-log radiative corrections to the running quartic Higgs self-couplings. We impose supersymmetric boundary conditions at $\mu=M_{\rm SUSY}$, the scale which characterizes the typical size of supersymmetry-breaking masses (e.g., squark and gaugino masses). At $\mu=M_{\rm SUSY}$, these couplings are related to gauge couplings. We then use renormalization group equations to run the Higgs self-couplings and gauge couplings down to $\mu=m_t$. Finally, we decouple the top-quark and run the couplings down to m_Z. We can then express the physical-Higgs-boson masses and self-couplings in terms of the Higgs-boson self-couplings evaluated at m_Z. We diagonalize the radiatively corrected *CP*-even Higgs-boson mass matrix to obtain the mixing angle α, which appears in the couplings of the Higgs boson to the quarks, leptons, and gauge bosons. Details of this procedure and the relevant formulas can be found in Ref. [26].

We compute the A^0 branching ratios as a function of m_A for various choices of $\tan\beta$ and m_t. For illustrative purposes, the scale of supersymmetry breaking (e.g., the common squark mass) is taken to be $M_{\rm SUSY}=1$ TeV, and $\tilde{t}_L$-$\tilde{t}_R$ mixing is neglected. It is expected that $1\lesssim\tan\beta\lesssim m_t/m_b$ [28], so we have chosen two representative values: $\tan\beta=2$ and 20. We will present results for $m_t=150$ and 200 GeV. Finally, we note that the QCD corrections to Higgs decay to $Q\bar{Q}$ ($Q=c$, b, and t) have been included [19]. Our results are shown in Figs. 4 and 5.

We briefly note a number of important features of these results. We consider first the $\tan\beta=2$ results, typical of those obtained for moderate $\tan\beta$ values. From Fig. 4 we see that the $b\bar{b}$ mode is dominant (with $B\simeq 90\%$) for $m_A<m_Z+m_h$. In this same mass range the $\tau^+\tau^-$ mode has $B\sim 10\%$. For $m_Z+m_h<m_A<2m_t$, the $b\bar{b}$ and Zh^0 modes are competitive. As m_t increases, $B(A^0\to Zh^0)$ increases slightly due to the effects of radiative corrections to $\cos(\beta-\alpha)$ [see Eq. (16) and Fig. 3]. The shift in the $A^0\to Zh^0$ decay threshold to higher m_A as m_t increases is easily understood, since, for large m_t, the radiative corrections to m_h are substantial, as noted above. Very roughly speaking, for $m_t\sim 150$

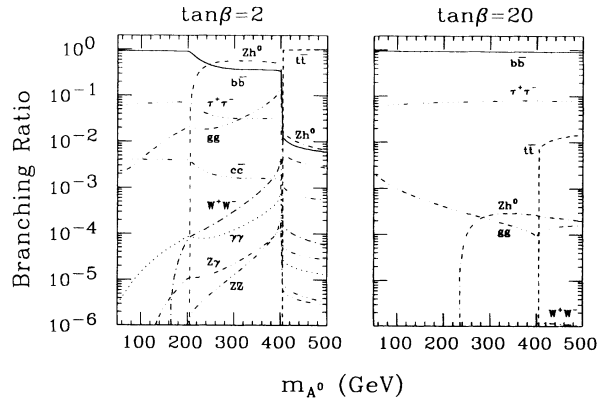

FIG. 5. Branching ratios for A^0 computed for $m_t=200$ GeV and for $\tan\beta=2$ and 20. One loop radiative corrections have been included as described in the text. The notation for the curves is that specified in the caption for Fig. 4.

GeV, $m_h = O(m_Z)$ for $m_A > m_h$, and m_h increases substantially above m_Z (for $\tan\beta \gtrsim 2$) as m_t gets larger, as shown in Fig. 2. For $m_A > 2m_t$, the $t\bar{t}$ decay mode is dominant as expected, since (at tree-level)

$$\frac{\Gamma(A^0 \to t\bar{t})}{\Gamma(A^0 \to b\bar{b})} \simeq \frac{m_t^2 \cot^4\beta}{m_b^2} \left[1 - \frac{4m_t^2}{m_A^2}\right]^{1/2}. \tag{17}$$

Finally, we note that the one-loop induced decays of A^0 to VV are rather small, although they peak sharply in the vicinity of $m_A = 2m_t$ (where the t-loop contribution is most important). In this region, the VV decay modes may be of phenomenological relevance. Here, it is important to note that the branching ratios of the VV modes depend very sensitively on $\tan\beta$, as shown in Fig. 6.

For $\tan\beta = 20$ (see Fig. 5) the $b\bar{b}$ mode is always dominant with $B \simeq 90\%$, followed by the $\tau^+\tau^-$ mode with $B \simeq 10\%$. Note that even when the $t\bar{t}$ mode is kinematically allowed, it never contributes more than a few percent of the branching ratio. This is easily understood from Eq. (17); in particular, $B(A^0 \to t\bar{t}) \lesssim B(A^0 \to b\bar{b})$ when $\tan\beta \gtrsim \sqrt{m_t/m_b}$. The Zh^0 branching ratio is greatly suppressed at large $\tan\beta$. This follows easily from Eq. (16) due to the factor of $\tan^2\beta$ in the denominator. [In addition, $\cos^2(\beta-\alpha)$ also decreases as $\tan\beta$ increases; see Fig. 3.] Finally, it is apparent that the one-loop induced VV modes are completely negligible at large $\tan\beta$ due to the $\cot^4\beta$ dependence in Eqs. (11)–(14), as shown in Fig. 6.

In the next section, we will make use of the branching ratio to ZZ. In Sec. V, we will comment on some of the implications of the other decay modes for A^0 searches at the SSC and LHC.

IV. THE GOLD-PLATED FOUR-LEPTON DISCOVERY CHANNEL

In this section, we present our computations for the number of $4l$ events resulting from A^0 production and decay at the SSC and LHC, including one-loop radiative corrections to the MSSM Higgs sector. Since $A^0 \to ZZ$ is a one-loop induced process, the event rate is expected to be rather meager. As we shall see, detection via this mode is only possible in a limited region of parameter space. The results of Sec. III suggest a region of $\tan\beta$ not larger than 2 and a limited region of A^0 masses near but below $t\bar{t}$ threshold, where $\Gamma(A^0 \to ZZ)$ is maximal. In our computations, we again consider $m_t = 150$ and $m_t = 200$ GeV and adopt supersymmetric parameters as specified in Sec. III.

In computing production cross section for the A^0 we have included three processes: $gg \to A^0$, $gg \to b\bar{b}A^0$, and $gg \to t\bar{t}A^0$. The latter is always much smaller than $gg \to A^0$, but will be included in our final $4l$ event rates for completeness. However, the $gg \to t\bar{t}A^0$ cross section may be useful on its own for other possible A^0 detection techniques. We shall present separately the cross section (without cuts) for the dominant $gg \to A^0$ and $gg \to b\bar{b}A^0$ fusion processes, as well as that for the $gg \to t\bar{t}A^0$ reaction. The $gg \to A^0 b\bar{b}$ cross section has been computed in the $b\bar{b}$ fusion approximation valid in the limit $m_A \gg 2m_b$.[5] In this calculation, $\sigma(b\bar{b} \to A^0)$ is proportional to the width $\Gamma(A^0 \to b\bar{b})$, which has been computed including the QCD corrections of Ref. [19]. The effect of these QCD corrections is to reduce $\sigma(b\bar{b} \to A^0)$ by about a factor of 2 due to the falloff of the running b-quark mass for $m_A \gg 2m_b$. The $gg \to t\bar{t}A^0$ process has been computed at the tree level. Results will only be presented for $\tan\beta = 1$. Since the $A^0 t\bar{t}$ coupling is proportional to $\cot\beta$, results for other $\tan\beta$ values can be obtained by scaling by $\cot^2\beta$.

Numerical results for the various cross sections (before cuts) at the SSC and LHC are presented in Figs. 7–10.[6] Clearly, the combined cross sections are very substantial, although those for the LHC energy of $\sqrt{s} = 16$ TeV are a factor of 4 to 5 smaller than the cross sections for the SSC energy of $\sqrt{s} = 40$ TeV. It is important to note that for large $\tan\beta$ the net cross section can actually be larger than for moderate $\tan\beta$, especially for smaller m_A. This arises from two effects: $\sigma(gg \to A^0 b\bar{b})$ is enhanced because the $A^0 b\bar{b}$ coupling is proportional to $\tan\beta$; whereas the t-*loop* contribution to $\sigma(gg \to A^0)$ is suppressed because the $A^0 t\bar{t}$ coupling is proportional to $\cot\beta$ [29].

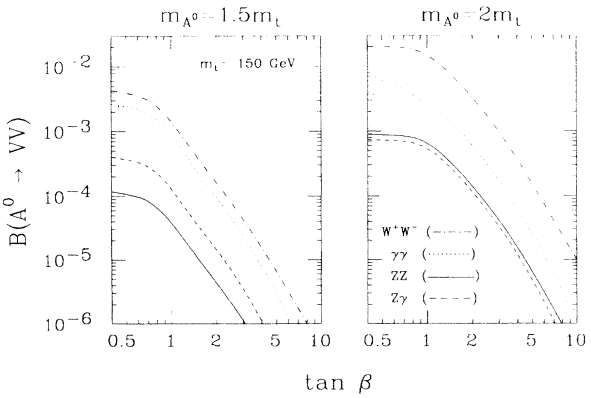

FIG. 6. Branching ratios for A^0 computed for $m_t = 150$ GeV as a function of $\tan\beta$ for $m_A = 1.5m_t$ and $2m_t$. One-loop radiative corrections have been included as described in the text. The notation for the curves is indicated in the figure (and differs slightly from that used in the previous two figures).

[5] In fact, the $b\bar{b}$ fusion approximation overestimates the cross section somewhat, particularly in the A^0 mass range below 500 GeV (e.g., see Ref. [29]). However, we have also not included the effects of higher order QCD corrections, which are often summarized by a multiplicative K factor larger than 1.

[6] We have employed the Eichten-Hinchliffe-Lane-Quigg (EHLQ) distributions for $\Lambda_{\overline{\rm MS}} = 0.29$ GeV [30] where $\overline{\rm MS}$ denotes the modified minimal subtraction scheme. For consistency, we used the same $\Lambda_{\overline{\rm MS}}$ value in evaluating the running strong coupling constant (g_s). The distribution functions and g_s were evaluated at $\hat{s}$, the subprocess center-of-mass energy squared. No QCD K factors have been included in the subprocess cross sections.

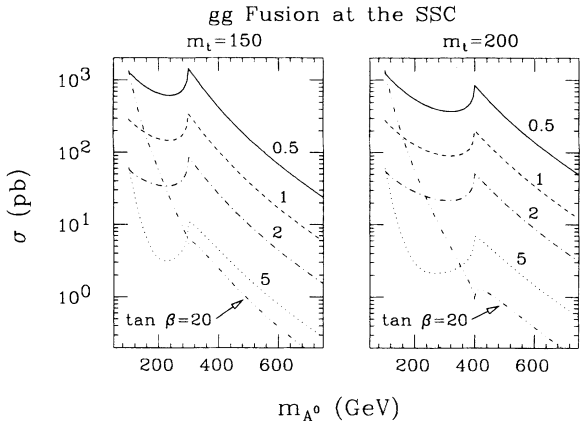

FIG. 7. The $pp \to A^0 + X$ cross sections from $gg \to A^0$ at the SSC for $m_t = 150$ and 200 GeV, for $\tan\beta = 0.5$ (——); $\tan\beta = 1$ (— — —); $\tan\beta = 2$ (—·—·—·); $\tan\beta = 5$(· · · ·); and $\tan\beta = 20$(··—··—).

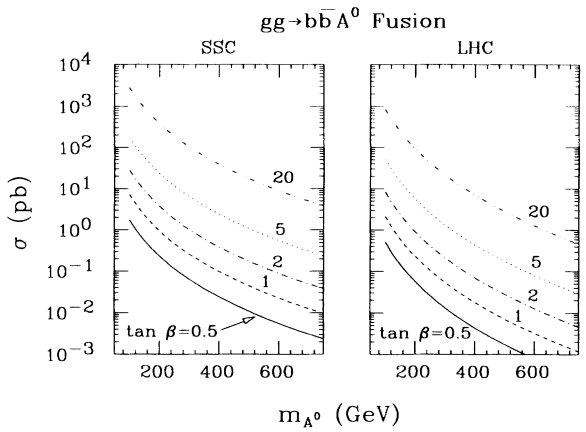

FIG. 9. The $pp \to A^0 b\bar{b} + X$ cross section from $gg \to A^0 b\bar{b}$ at the SSC and LHC for $m_t = 150$ GeV, for $\tan\beta = 0.5$(——); $\tan\beta = 1$(— — —); $\tan\beta = 2$(—·—·—·); $\tan\beta = 5$(· · · ·); and $\tan\beta = 20$(··—··—). Variation with m_t is very minimal.

Using these cross sections, we have computed event rates in the $4l$ mode (summing over the possible electron and muon channels) at both the LHC and SSC for an integrated luminosity of $L = 30$ fb^{-1}. This choice of L is made on the basis that it is a reasonable expectation for three years running at the SSC. We have estimated the effects of realistic detector cuts and efficiencies as described in detail in Ref. [8]. Following the analysis of Ref. [8], we shall multiply the raw signal (and background) rates by a net efficiency factor of $\epsilon = 0.35$.

The only significant background process to the $4l$ signal is $q\bar{q}, gg \to ZZ \to 4l$ [31]. Other backgrounds are much smaller once the isolation and other cuts incorporated in the above efficiency factor are imposed. The number of background events at the SSC and LHC is determined as described in Ref. [8]. In particular, it is necessary to know what resolution in the $4l$ invariant mass is possible. We shall give results for two extreme assumptions. First, we consider the conservative values of $\Gamma^{\rm res} = 4.8$ GeV at $m_{4l} = 200$ GeV and $\Gamma^{\rm res} = 14.0$ GeV at $m_{4l} = 400$ GeV. ($\Gamma^{\rm res}$ for other invariant masses is obtained by linear interpolation or extrapolation.) We shall also give results for the technically feasible, but certainly optimistic, choices of $\Gamma^{\rm res} = 2.2$ GeV at $m_{4l} = 200$ GeV and $\Gamma^{\rm res} = 5.1$ GeV at $m_{4l} = 400$ GeV. The conservative and optimistic possibilities for $\Gamma^{\rm res}$ are labeled below by I and II, respectively. In computing the signal versus background rates, we shall integrate over a bin size of $2\Gamma^{\rm res}$ in order to include essentially 100% of the signal events coming from the (very narrow) Higgs resonance.

Our results for the A^0 are summarized in a series of figures. First, we consider results obtained for the SSC. In Figs. 11 and 12 we display the $4l$ event rates (including the efficiency factor of $\epsilon = 0.35$) from A^0 production and decay at the SSC with $L = 30$ fb^{-1}, for $m_t = 150$ and 200

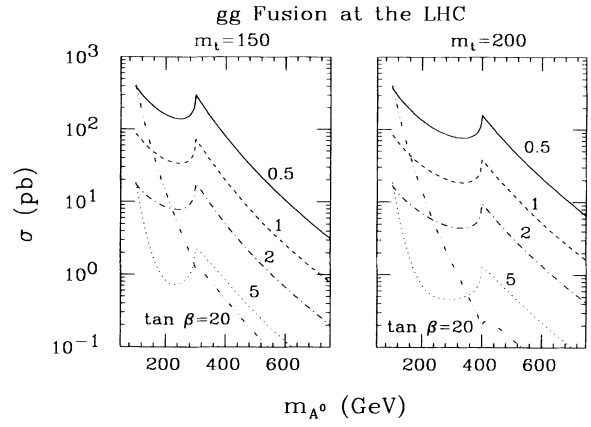

FIG. 8. The $pp \to A^0 + X$ cross sections from $gg \to A^0$ at the LHC for $m_t = 150$ and 200 GeV, for $\tan\beta = 0.5$ (——); $\tan\beta = 1$(— — —); $\tan\beta = 2$(—·—·—·); $\tan\beta = 5$(· · · ·); and $\tan\beta = 20$(··—··—). Note the change in scale from that of Fig. 7.

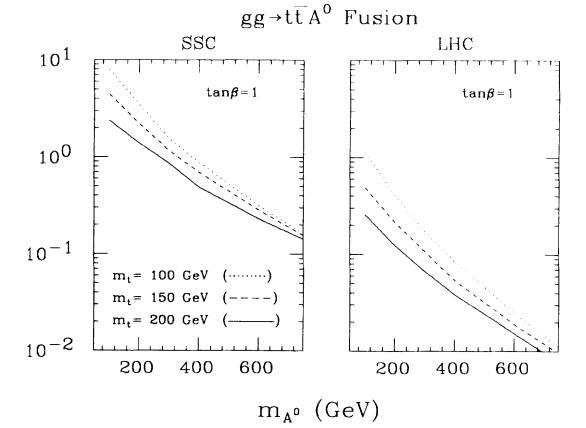

FIG. 10. The $pp \to A^0 t\bar{t} + X$ cross section from $gg \to A^0 t\bar{t}$ at the SSC and LHC for $m_t = 100$, 150, and 200 GeV, for $\tan\beta = 1$. Results for other $\tan\beta$ values can be obtained by scaling by $\cot^2\beta$.

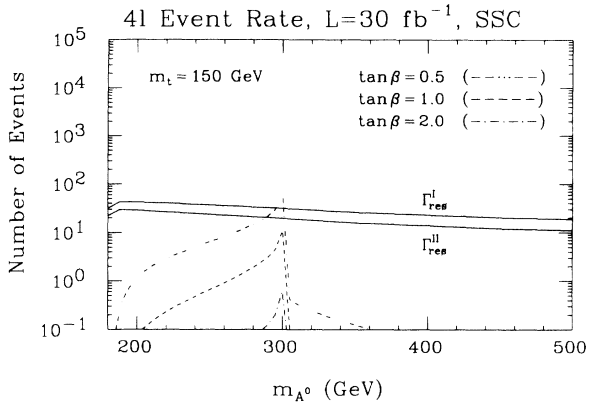

FIG. 11. $4l$ event rates for $L=30$ fb^{-1}, $\epsilon=0.35$, and $m_t=150$ GeV at the SSC, compared to the minimum number required for a 4σ effect. The $H^0\to 4l$ signal curves are $\tan\beta=0.5$ ($\cdots--$), $\tan\beta=1$($---$), and $\tan\beta=2$ ($-\cdot-\cdot-$). The two 4σ curves (——) correspond to $\Gamma_{\rm I}^{\rm res}$ and $\Gamma_{\rm II}^{\rm res}$ (see text). Other supersymmetric model parameters are specified in the text.

GeV, respectively. Results for various values of $\tan\beta$ are illustrated. Also displayed is the minimum event number as a function of mass that is required to obtain a 4σ statistical significance,[7] assuming the conservative and optimistic $4l$ mass resolution $\Gamma_{\rm I}^{\rm res}$ and $\Gamma_{\rm II}^{\rm res}$. From these two figures, it is evident that the A^0 can generally be detected via its $4l$ decays only for $\tan\beta\lesssim 1$ and only in a very narrow mass region in the vicinity of $m_A\sim 2m_t$.

Of course, these figures can easily be adjusted for different possible values of the accumulated luminosity L.

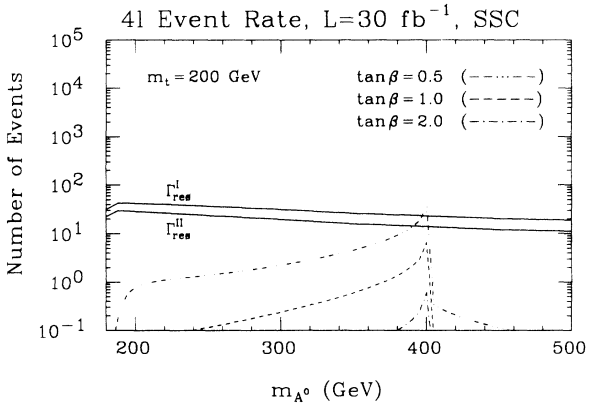

FIG. 12. $4l$ event rates for $L=30$ fb^{-1}, $\epsilon=0.35$, and $m_t=200$ GeV at the SSC, compared to the minimum number required for a 4σ effect. Notation as in Fig. 11.

[7]We choose to use $S/\sqrt{B}$ as a criterion rather than $S/\sqrt{S+B}$ since it is probable that B will be well determined from the background measured away from the Higgs-boson resonance peak region.

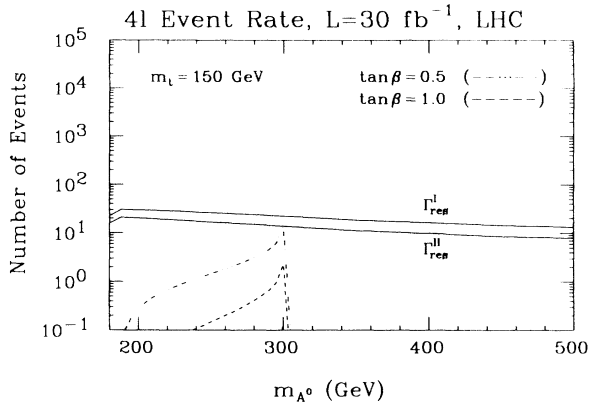

FIG. 13. $4l$ event rates for $L=30$ fb^{-1}, $\epsilon=0.35$, and $m_t=150$ GeV at the LHC, compared to the minimum number required for a 4σ effect. Notation as in Fig. 11. The $\tan\beta=2$ event rate is too small to appear on the figure.

If only $L=10$ fb^{-1} is available, then detection limits for the $A^0\to 4l$ can be read off by looking for the points at which the signal and minimum 4σ even rate curves cross *after* decreasing the signal event rate curves by a factor of $\sqrt{3}$ (equivalent to decreasing the signal curves by a factor of 3 and the minimal 4σ event rate curves by a factor of $\sqrt{3}$). By performing this exercise, one easily sees that, with only $L=10$ fb^{-1}, a 4σ signal in $S/\sqrt{B}$ for $A^0\to 4l$ would not be achieved even for $m_A\sim 2m_t$ for $\tan\beta\gtrsim 0.5$.

At the LHC, event rates for $A^0\to 4l$ are typically smaller by a factor of about 5, depending upon Higgs mass (see, in particular, Figs. 7, 8, and 9). Meanwhile, the $ZZ\to 4l$ continuum background decreases only by roughly a factor of 2, implying a factor of $\sqrt{2}$ decrease in the 4σ event level criterion. These results are illustrated in Figs. 13 and 14. Clearly, there is no region of parameter space for which a 4σ effect in the $A^0\to 4l$ mode emerges at the LHC. At $L=100$ fb^{-1} one is just on the borderline of achieving a 4σ signal at $m_A=2m_t$ if $\tan\beta\lesssim 0.5$.

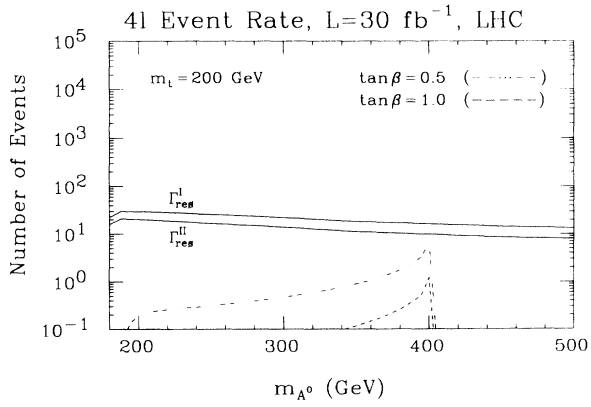

FIG. 14. $4l$ event rates for $L=30$ fb^{-1}, $\epsilon=0.35$, and $m_t=200$ GeV at the LHC, compared to the minimum number required for a 4σ effect. Notation as in Fig. 11. The $\tan\beta=2$ event rate is too small to appear on the figure.

Fortunately, the $4l$ mode is not the only means by which the SSC and LHC might be sensitive to the MSSM Higgs sector. We now turn to a survey of other possible scenarios for detection of the A^0.

V. OTHER CHANNELS FOR A^0 HIGGS-BOSON DETECTION

Clearly, the very marginal utility of the $4l$ mode for detection of the *CP*-odd neutral Higgs boson of the MSSM mandates an examination of other production/decay scenarios that might permit its discovery. It follows from Fig. 6 that some of the other one-loop induced VV decay modes of the A^0 have substantially larger branching ratio than the $A^0 \to ZZ \to 4l$ mode, and that these decays might be useful for $\tan\beta \lesssim 1-2$. Perhaps the most important VV signature is the detection of A^0 via its two-photon decay mode [9,12]. In Ref. [9], $gg \to t\bar{t}A^0$ followed by $t \to Wb \to l\nu b$ and $A^0 \to \gamma\gamma$ is shown to be detectable in a significant range of parameter space, extending from $m_A \sim m_Z$ up to $m_Z \sim 2m_t$ for $\tan\beta \lesssim 2$. One could also consider the possibility of searching for $A^0 \to W^+W^- \to e^{\pm}\mu^{\mp} + X$. However, even for small $\tan\beta$ and the most optimal A^0 mass choice, $m_A = 2m_t$, Fig. 6 shows that the net branching ratio for such final states is

$$B(A^0 \to W^+W^- \to e^{\pm}\mu^{\mp} + X) \lesssim 2 \times 10^{-2} \times 2 \times (\tfrac{1}{9})^2 \simeq 5 \times 10^{-4} . \quad (18)$$

For other m_A values or larger $\tan\beta$ this branching ratio is much smaller. In fact, as discussed below, $A^0 \to \tau^+\tau^-$ decays always lead to a much larger rate for $e^{\pm}\mu^{\mp} + X$ final states, especially at large $\tan\beta$. More generally, since neither the $4l$ nor the $l\nu\gamma\gamma$ final states allow any sensitivity to the $\tan\beta \gtrsim 2$ region of parameter space, it is crucial to consider the other channels that might allow A^0 detection, particularly at larger $\tan\beta$ values.

Thus, we turn to other decay channels depicted in the branching ratio curves of Sec. III. Foremost among these is the $\tau^+\tau^-$ decay mode, which is generally quite significant except in the region above $t\bar{t}$ threshold when $\tan\beta \lesssim 5$. From Figs. 4 and 5, we see that $B(A^0 \to \tau^+\tau^-)$ is typically close to 10% at large $\tan\beta$ for all m_A, and ranges between about 5% and 9% when $\tan\beta \sim 2$ and $m_A < 2m_t$. Thus,

$$B(A^0 \to \tau^+\tau^- \to e^{\pm}\mu^{\mp} + X) \lesssim 0.1 \times 2 \times (0.177)^2 \simeq 6.3 \times 10^{-3} . \quad (19)$$

If one searches for $e^{\pm}\mu^{\mp} + X$ (where both leptons are isolated), the main background will be from $t\bar{t}$ production followed by the decay of the resulting W^+W^- to the same final state. This background can be reduced by antitagging against the extra jets present in the $t\bar{t}$ process, etc. The main problem is that in the inclusive production of the A^0 only approximate reconstruction of the A^0 mass will be possible (using a high-p_T jet or similar tag). Some studies of the $\tau^+\tau^-$ mode for the case of the standard model Higgs boson have been performed for the LHC (see Ref. [32]), and implications of these studies for the $A^0 \to \tau^+\tau^-$ detection mode were outlined by Kunszt and Zwirner in Ref. [12].

Finally, we briefly survey a number of other possible A^0 signatures. For $m_Z + m_h < m_A < 2m_t$, the $A^0 \to Zh^0 \to l^+l^-b\bar{b}$ final state has substantial branching ratio, and could provide a viable signal [1,2,12]. For example, at $\tan\beta = 2$ and for $m_t = 150$ GeV we find from Fig. 4 that

$$B(A^0 \to Zh^0 \to l^+l^-b\bar{b}) \lesssim 0.45 \times 0.066 \simeq 3 \times 10^{-2} \quad (20)$$

in the specified range of m_A. If efficient b tagging is possible, the principal background will be from $Zb\bar{b}$ associated production. This background may be manageable, assuming that reconstruction of the h^0 and A^0 mass peaks in the $b\bar{b}$ and $Zb\bar{b}$ channels, respectively, is possible with reasonable resolution.

For $m_A > 2m_t$, $A^0 \to Zh^0$ is never a significant decay mode. Moreover, for $\tan\beta \lesssim 4$, $A^0 \to t\bar{t}$ is dominant, and probably the only viable technique would be to search for $t\bar{t}A^0$ associated production, followed by $A^0 \to t\bar{t}$. The $t\bar{t}t\bar{t}(4t)$ continuum background cross section is of similar size to the $4t$ rate obtained from the Higgs-boson signal [33]. Consequently, if one could efficiently trigger on the $4t$ final state in such a way as to eliminate the many (much larger) reducible backgrounds, isolation of a signal for the A^0 in this channel might be possible.

Associated $W + A^0$ production, followed by $W \to l\nu$ and $A^0 \to \tau^+\tau^-$ or $A^0 \to Zh^0$, may also provide a useful signature. However, it should be noted that the absence at tree level of the WWA^0 vertex and the suppression at large $\tan\beta$ of the $A^0t\bar{t}$ associated production process imply that this detection mode will only be useful if $\tan\beta$ is not much larger than 1. Similarly, associated $Z + A^0$ production followed by $Z \to l^+l^-$ and $A^0 \to \tau^+\tau^-$ or $A^0 \to Zh^0$ may provide an observable signal over background if sufficient integrated luminosity is accumulated [34].

All of the above possibilities are currently under investigation.

VI. CONCLUSIONS

In this paper we have presented a detailed survey of the phenomenology of the *CP*-odd Higgs boson, A^0, of the MSSM. A comprehensive set of A^0 decay branching ratios has been obtained for all two-body nonsupersymmetric final states, and the major A^0 production mechanisms have been reevaluated. Our results incorporate one-loop leading-log radiative corrections to the MSSM Higgs sector parameters. In addition, the widths and branching ratios for the one-loop decays $A^0 \to VV$ for all possible vector boson pair final states have been obtained. Using the results, we have evaluated the signal and background rate for detection of A^0 in the one-loop induced $A^0 \to ZZ \to l^+l^-l^+l^-$ decay mode. We find that the $A^0 \to 4l$ mode will only be a useful discovery channel at the SSC or LHC if $\tan\beta$ is small ($\lesssim 1$) and m_A is near the $t\bar{t}$ threshold. Fortunately, our survey of a variety of other possible production/decay modes reveals a number of promising techniques for detecting the A^0 at a hadron supercollider. These techniques will require further

study, including realistic background analysis and detector simulations, in order to truly assess their viability for A^0 discovery.

ACKNOWLEDGMENTS

This project originated at the U.C. Davis Workshop on Higgs/EWSB Physics at Hadron Supercolliders. We would like to thank A. Mendez for a number of illuminating discussions. One of us (C.K.) would like to thank Duane Dicus for beneficial discussions and comments. Two of us (J.F.G. and H.E.H.) acknowledge the hospitality of the Aspen Center for Physics where part of this work was completed. This work was supported in part by the Department of Energy.

APPENDIX

The results of the one-loop calculation of $A^0 \to V_i V_j$ can be expressed in terms of two functions $\mathcal{C}$ and $\mathcal{F}$. It is convenient to make use of the 't Hooft–Veltman scalar loop integrals [16] defined below. However, in contrast with Ref. [16], we employ the metric conventions of Bjorken and Drell [35]. We define

$$C_0(k_1^2,k_2^2,k^2;m_a^2,m_b^2,m_c^2) = -16\pi^2 i \int \frac{d^4q}{(2\pi)^4}\frac{1}{\mathcal{D}} ,$$
$$C^\mu(k_1^2,k_2^2,k^2;m_a^2,m_b^2,m_c^2) = -16\pi^2 i \int \frac{d^4q}{(2\pi)^4}\frac{q^\mu}{\mathcal{D}} , \tag{A1}$$

where

$$\mathcal{D} = (q^2-m_a^2)[(q+k_1)^2-m_b^2][(q+k_1+k_2)^2-m_c^2] , \tag{A2}$$

and $k = k_1 + k_2$ is the momentum of the A^0. By Lorentz invariance,

$$C^\mu = C_{11}k_1^\mu + C_{12}k_2^\mu . \tag{A3}$$

We now define the two functions

$$\mathcal{C}(m_{V_i}^2,m_{V_j}^2;m_t^2,m_b^2) \equiv C_0(m_{V_i}^2,m_{V_j}^2,m_A^2;m_t^2,m_b^2,m_t^2) , \tag{A4}$$

$$\mathcal{F}(m_{V_i}^2,m_{V_j}^2;m_t^2,m_b^2) \equiv C_{11}(m_{V_i}^2,m_{V_j}^2;m_A^2;m_t^2,m_b^2,m_t^2) - C_{12}(m_{V_i}^2,m_{V_j}^2,m_A^2;m_t^2,m_b^2,m_t^2) .$$

For ease of notation, we have suppressed m_A^2 in the arguments on the left-hand side above. In addition, in the case of equal masses, we shall simplify our notation by not repeating the corresponding mass in the list of arguments. For example,

$$\mathcal{C}(m_V^2;m_t^2,m_b^2) \equiv \mathcal{C}(m_V^2,m_V^2;m_t^2,m_b^2) ,$$
$$\mathcal{C}(m_{V_i}^2,m_{V_j}^2;m_t^2) \equiv \mathcal{C}(m_{V_i}^2,m_{V_j}^2;m_t^2,m_t^2) , \tag{A5}$$

and similarly for $\mathcal{F}$.

TABLE II. Asymptotic forms for loop functions in the limit of $m_t \gg m_A, m_V$.

Function	Large-m_t results
$\mathcal{C}(m_V^2;m_t^2,m_b^2)$	$\frac{-1}{m_t^2}$
$\mathcal{C}(m_V^2;m_b^2,m_t^2)$	$\frac{-1}{m_t^2}\left[\ln\left[\frac{-m_t^2}{m_A^2}\right]+1\right]$
$\mathcal{C}(m_V^2,0;m_t^2)$	$\frac{-1}{2m_t^2}$
$\mathcal{C}(m_V^2;m_t^2)$	$\frac{-1}{2m_t^2}$
$\mathcal{F}(m_V^2;m_t^2,m_b^2)$	$\frac{1}{2m_t^2}$
$\mathcal{F}(m_V^2;m_b^2,m_t^2)$	$\frac{1}{2m_t^2}$
$\mathcal{F}(m_V^2;m_t^2)$	$\frac{1}{6m_t^2}$

All these functions can be easily evaluated numerically using the techniques described in Ref. [16]. For the cases of $A^0 \to \gamma\gamma$ and $A^0 \to Z\gamma$, the evaluation of the loop integrals greatly simplifies. It is easy to show that

$$\mathcal{C}(0;m_f^2) = \frac{1}{m_A^2}\int_0^1 \frac{dx}{x}\ln\left[1-\frac{4x(1-x)}{\tau_A}\right] \equiv \frac{-2}{m_A^2}f(\tau_A) , \tag{A6}$$

where $\tau_X \equiv 4m_f^2/m_X^2$ and

$$f(\tau) = \begin{cases} [\arcsin(\sqrt{1/\tau})]^2 & \text{if } \tau \geq 1, \\ -\frac{1}{4}\left[\ln\left[\frac{1+\sqrt{1-\tau}}{1-\sqrt{1-\tau}}\right]-i\pi\right]^2 & \text{if } \tau < 1 . \end{cases} \tag{A7}$$

By a similar calculation,

$$\mathcal{C}(m_Z^2,0;m_f^2) = \mathcal{C}(0,m_Z^2;m_f^2) = \frac{-2}{m_A^2-m_Z^2}[f(\tau_A)-f(\tau_Z)] . \tag{A8}$$

We now turn to asymptotic forms for the loop functions in the limit of large m_t. These are most easily obtained from the integral representations

$$\mathcal{C}(m_{V_i}^2,m_{V_j}^2;m_t^2,m_b^2) \equiv \int_0^1 dx \int_0^x dy \frac{1}{D} ,$$
$$\mathcal{F}(m_{V_i}^2,m_{V_j}^2;m_t^2,m_b^2) \equiv -\int_0^1 dx \int_0^x y\, dy \frac{1}{D} , \tag{A9}$$

where

$$D \equiv m_A^2(1-x)(x-y) + m_{V_i}^2 y(1-x) + m_{V_j}^2 y(x-y) - m_t^2(1-y) - m_b^2 y . \tag{A10}$$

The required asymptotic forms are listed in Table II.

[1] J. F. Gunion, H. E. Haber, G. Kane, and S. Dawson, *The Higgs Hunter's Guide* (Addison-Wesley, Redwood City, CA, 1990).

[2] J. F. Gunion *et al.*, in *Research Directions for the Decade,* Proceedings of the Snowmass Summer Study on High Energy Physics, Snowmass, Colorado, 1990, edited by E. L. Berger and I. Butler (World Scientific, Singapore, 1991).

[3] J. F. Gunion, in Proceedings of the Workshop in High Energy Physics Phenomenology—II, Calcutta, 1991 (unpublished).

[4] Z. Kunszt and W. J. Stirling, in *Proceedings of the ECFA Large Hadron Collider Workshop,* Aachen, Germany, 1990, edited by G. Jarlskog and D. Rein (CERN Report No. 90-10, Geneva, Switzerland, 1990), Vol. II, p. 428; D. Froidevaux, *ibid.*, p. 444.

[5] E. Witten, Nucl. Phys. **B188**, 513 (1981); S. Dimopoulous and H. Georgi, *ibid.* **B193**, 150 (1981); N. Sakai, Z. Phys. C **11**, 153 (1981).

[6] K. Inoue, A. Kakuto, H. Komatsu, and S. Takeshita, Prog. Theor. Phys. **67**, 1889 (1982); **68**, 927 (1982); **70**, 330(E) (1983); **71**, 413 (1984); R. Flores and M. Sher, Ann. Phys. (N.Y.) **148**, 95 (1983).

[7] J. F. Gunion and H. E. Haber, Nucl. Phys. **B272**, 1 (1986); **B278**, 449 (1986).

[8] J. F. Gunion, R. Bork, H. E. Haber, and A. Seiden, Phys. Rev. D **46**, 2040 (1992).

[9] J. F. Gunion and L. Orr, Phys. Rev. D **46**, 2052 (1992).

[10] ALEPH Collaboration, D. Decamp *et al.*, Phys. Lett. B **237**, 291 (1990); **265**, 475 (1991); DELPHI Collaboration, P. Abreu *et al.*, *ibid.* **245**, 276 (1990); Nucl. Phys. **B373**, 3 (1992); L3 Collaboration, B. Adeva *et al.*, Phys. Lett. B **251**, 311 (1990); OPAL Collaboration, M. Z. Akrawy *et al.*, Z. Phys. C **49**, 1 (1991).

[11] J. F. Gunion *et al.*, Phys. Rev. D **38**, 3444 (1988).

[12] Z. Kunszt and F. Zwirner, in *Proceedings of the ECFA Large Hadron Collider Workshop* [4], p. 578; Report No. ETH-TH/91-7, 1991 (unpublished); V. Barger, M. S. Berger, A. L. Stange, and R. J. N. Phillips, Phys. Rev. D **45**, 4128 (1992); H. Baer, M. Bisset, C. Kao, and X. Tata, *ibid.* **46**, 1067 (1992).

[13] The decay widths for $A^0 \to W^+W^-$ and $A^0 \to ZZ$ (for $m_b = 0$) have been obtained independently by A. Mendez and A. Pomarol, Phys. Lett. B **272**, 313 (1991).

[14] See Ref. [1], pp. 197–199.

[15] V. Barger *et al.*, Phys. Rev. D **35**, 3366 (1987); **38**, 1632(E) (1988).

[16] G. 't Hooft and M. Veltman, Nucl. Phys. **B153**, 365 (1979); G. Passarino and M. Veltman, *ibid.* **B160**, 151 (1979).

[17] J. F. Gunion, G. Gamberini, and S. Novaes, Phys. Rev. D **38**, 3481 (1988).

[18] T. J. Weiler and T.-C. Yuan, Nucl. Phys. **B318**, 337 (1989).

[19] M. Drees and K. Hikasa, Phys. Lett. B **240**, 455 (1990); **262**, 497(E) (1991).

[20] G. Pócsik and G. Zsigmond, Phys. Lett. **112B**, 157 (1982).

[21] H. E. Haber and R. Hempfling, Phys. Rev. Lett. **66**, 1815 (1991).

[22] J. Ellis, G. Ridolfi, and F. Zwirner, Phys. Lett. B **257**, 83 (1991); **262**, 477 (1991); A. Brignole, J. Ellis, G. Ridolfi, and F. Zwirner, *ibid.* **271**, 123 (1991).

[23] Y. Okada, M. Yamagushi, and T. Yanagida, Prog. Theor. Phys. **85**, 1 (1991); Phys. Lett. B **262**, 54 (1991).

[24] R. Barbieri, M. Frigeni, and F. Caravaglios, Phys. Lett. B **258**, 167 (1991); R. Barbieri and M. Frigeni, *ibid.* **258**, 395 (1991).

[25] A. Yamada, Phys. Lett. B **263**, 395 (1991); D. M. Pierce, A. Papadopoulos, and S. Johnson, Phys. Rev. Lett. **68**, 3678 (1992); K. Sasaki, M. Carena, and C. E. M. Wagner, Report No. MPI-Ph/91-109, 1991 (unpublished).

[26] H. E. Haber, in *Proceedings of the International Workshop on Electroweak Symmetry Breaking,* Hiroshima, Japan, 1991 (World Scientific, Singapore, in press); H. E. Haber and R. Hempfling, SCIPP Report No. SCIPP-91/33, 1991 (unpublished).

[27] P. H. Chankowski, S. Pokorski, and J. Rosiek, Phys. Lett. B **274**, 191 (1992); A. Brignole, *ibid.* **281**, 284 (1992).

[28] See, e.g., G. F. Giudice and G. Ridolfi, Z. Phys. C **41**, 447 (1988); M. Olechowski and S. Pokorski, Phys. Lett. B **214**, 393 (1988); M. Drees and M. M. Nojiri, Nucl. Phys. **B369**, 54 (1992).

[29] D. A. Dicus and S. Willenbrock, Phys. Rev. D **39**, 751 (1989).

[30] E. Eichten, I. Hinchliffe, K. Lane, and C. Quigg, Rev. Mod. Phys. **56**, 579 (1984); **58**, 1065(E) (1986).

[31] R. Brown and K. Mikaelian, Phys. Rev. D **19**, 922 (1979); D. Dicus, C. Kao, and W. Repko, *ibid.* **36**, 1570 (1987); E. W. N. Glover and J. van der Bij, Nucl. Phys. **B321**, 561 (1989).

[32] L. DiLella, in *Proceedings of the ECFA Large Hadron Collider Workshop* [4], p. 530; K. Bos, F. Anselmo, and B. van Eijk, *ibid.* p. 538.

[33] Z. Kunszt, Nucl. Phys. **B247**, 399 (1984); V. Barger, A. Stange, and R. J. N. Phillips, Phys. Rev. D **44**, 1987 (1991).

[34] C. Kao, Report No. FSU-HEP-911205, 1991 (unpublished).

[35] J. D. Bjorken and S. D. Drell, *Relativistic Quantum Mechanics* (McGraw-Hill, New York, 1964).